Submicron Nanoporous Polymer Support Membrane for More Transmissive X-Ray Windows

Kendall Berry

A senior thesis submitted to the faculty of
Brigham Young University
in partial fulfillment of the requirements for the degree of

Bachelor of Science

Robert Davis and Richard Vanfleet, Advisors

Department of Physics and Astronomy

Brigham Young University

April 2016

Copyright © 2016 Kendall Berry

All Rights Reserved

ABSTRACT

Submicron Nanoporous Polymer Support Membrane for More Transmissive X-Ray Windows

Kendall Berry
Department of Physics and Astronomy, BYU
Bachelor of Science

X-ray spectroscopy effectively gives insight into material development and other fields by detecting characteristic x-ray emissions from a sample. Measurement of lower Z-number elements is limited by poor transmission through the detector-sample chamber interface, or x-ray window. A thinner, more transmissive window would allow detection of these elements, but it would also need additional support to withstand the required differential pressures. A process for fabricating submicron-thick nanoporous polymer support membranes was developed using electron beam lithography, thermal nickel evaporation, and reactive ion etching. Bulge testing the resulting films gave insight into material strength and properties. Preliminary results are inconclusive but seem to indicate that membranes similar to the ones fabricated here may be able to serve as support structures for more transmissive x-ray windows.

Keywords: Electron beam lithography, reactive ion etching, membrane, film, pores, bulge testing, x-ray windows, thermal evaporation

ACKNOWLEDGMENTS

Many thanks to Lei Pei for teaching me how to do electron beam lithography, to Joseph Rowley for building the bulge test apparatus and software and for training me on it and on the atomic force microscope, to Kevin Laughlin for training me on the thermal evaporator, to Kyle Larsen for modeling x-ray transmission and helping with bulge testing software, and to Jim Frasier for helping me on countless occasions in the cleanroom. Also thanks to Michael Standing, Jeff Farrer, and Paul Minson for help and training on the electron microscopes in the McDonald Building and Eyring Science Center. Funding was provided by the BYU Physics Department and Moxtek, Inc.

Contents

Table of Contents **iv**

1 Introduction **1**
1.1 Motivation 1
1.2 Window Requirements 3
1.3 Support Membrane 5

2 Methods **7**
2.1 Fabrication Overview 7
2.2 Substrate 7
2.3 Electron Beam Lithography 9
2.4 Thermal Evaporation 11
2.5 Reactive Ion Etching and Resist Removal 13
2.6 Bulge Testing 15

3 Results **18**
3.1 Patterned Film 18
3.2 Bulge Testing Results 19
3.3 Conclusions and Future Work 25

Index **27**

List of Figures **28**

Bibliography **29**

Chapter 1

Introduction

1.1 Motivation

In material development and analysis, energy-dispersive x-ray spectroscopy (EDX) gives insight into sample composition. The material is placed inside a scanning electron microscope (SEM) and taken to high vacuum. As the electron beam hits the sample, it expels electrons from the atoms' inner shells. Electrons from higher energy levels quickly fill the empty spots, emitting x-rays. The sets of various x-ray energies are unique to each element and map the allowed transitions in the material. With a detector, the energies of these characteristic x-rays can be measured and recorded. By identifying where the peaks are in the resulting spectrum, researchers can determine which elements are present in the sample.

The detector operates at very low temperatures, so it must be shielded from normal atmospheric conditions to prevent ice from forming. Therefore, because the SEM chamber frequently goes from atmosphere to high vacuum, there must be an interface between the detector and the chamber, an x-ray window. However, these windows are not perfectly transparent to x-rays; photons with energies below 0.1 keV are mostly all absorbed by x-ray windows in current use [1]. This means

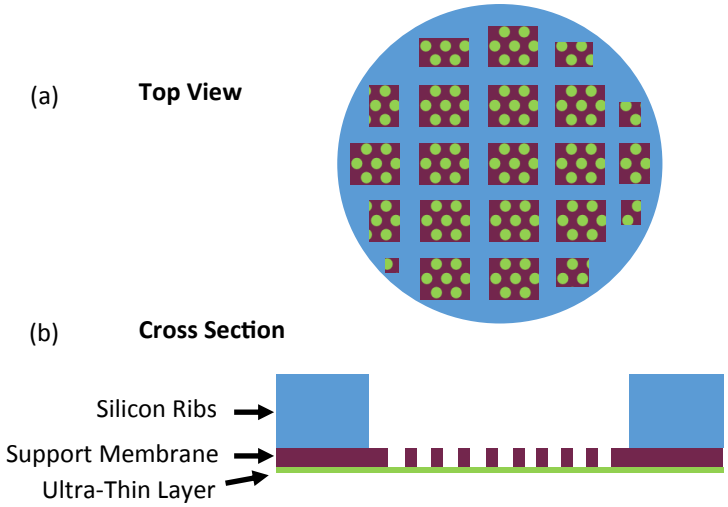


Figure 1.1 Schematic for a more transmissive x-ray window. The green (bottom in b) is the air-tight, ultra-thin, transmissive layer; the maroon (middle in b) is the support membrane that reduces the area the ultra-thin layer needs to span; and the blue areas (top in b) are the cross-ribs that support the other two layers.

that elements with low energy characteristic x-rays (low-Z elements like lithium or beryllium) are virtually impossible to detect. With improved transmission through the x-ray window, low-Z elements could be identified.

So how can transmission be increased? Transmission depends on material type and thickness. A thinner window composed of highly transmissive materials would allow detection of low-Z elements. The goal of this project is to prototype a membrane that could be part of a better x-ray window (see Fig 1.1). The overall window will have several layers: an ultra-thin, highly transmissive film; a porous membrane that supports that film by reducing the area it has to span; and support ribs that reduce the area the previous layers have to span. This project focused on developing the porous support membrane (see Fig 1.2).

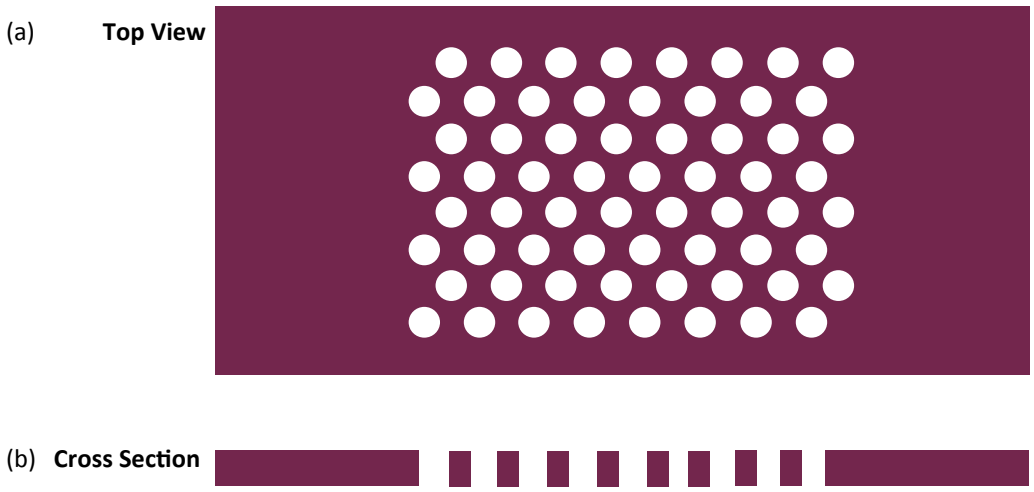


Figure 1.2 Support membrane schematic. The goal pattern is an area 100 μm x 100 μm filled with pores 200 nm in diameter, with 400 nm center-to-center spacing.

1.2 Window Requirements

A viable x-ray window must meet certain requirements. First, the materials that make up the window must be reasonably transparent to x rays. Second, the window must block visible wavelengths so that background noise does not overwhelm the signal [2]. Third, it must also hold pressure differentials experienced in handling, installation, and sample loading without leaking or breaking.

Because higher Z number window material means lower x-ray transmittance, material choices are usually restricted to beryllium, silicon nitride, and carbon-based compounds [1]. Beryllium is typically used for hand-held detectors because it transmits well and is robust and light-tight. However, at practical thicknesses, the transmission of energies below 0.5 keV is essentially zero (see Fig 1.3). Beryllium is also expensive and poses a health hazard. Many current x-ray windows used in SEM systems are made of polymers. While better than beryllium windows in terms of cost and safety, poor transmittance below 0.15 keV prohibits detection of beryllium or lithium [1] (see Fig 1.4).

Much x-ray window development has focused on graphenic carbon, such as the research done

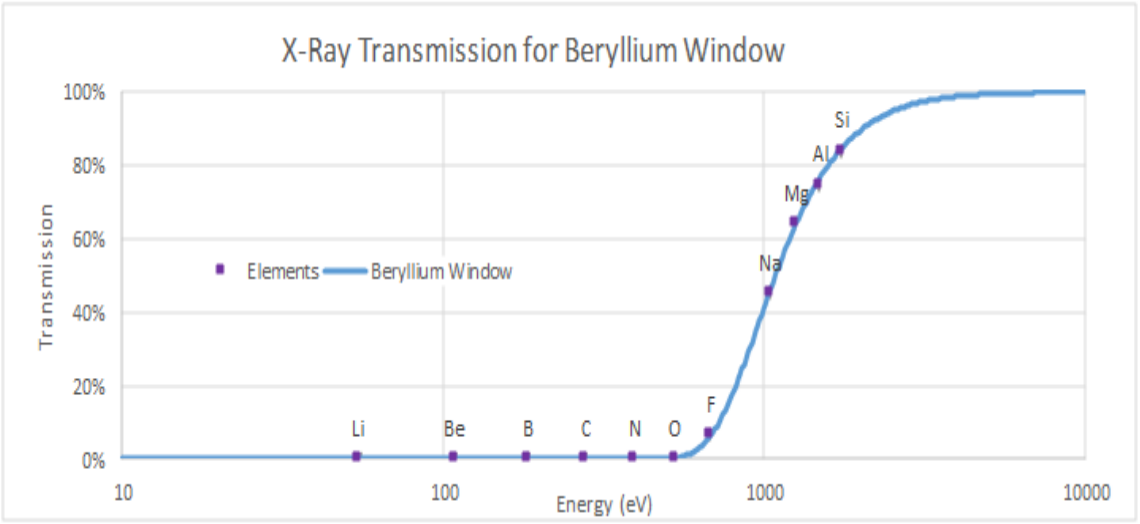


Figure 1.3 X-ray transmission for a typical 8 µm thick beryllium x-ray window. Transmission data courtesy of the Center for X-Ray Optics at Lawrence Berkeley National Labs.

by Huebner et al [3]. They fabricated 1 μm thick multi-layer graphene windows that spanned 5 mm, held pressure, and had better transmittance than beryllium. However, transmission at low energies was still not good enough. Graphenic carbon is promising, but for transmittance to reach desired levels, the window must be thinner.

Because the detector window is exposed to atmospheric pressure again and again, it needs to withstand at least 1 atm over many cycles. In practice, detector handling and installation may induce pressures higher than this, so 2 atm is the benchmark [3]. A window thin enough for the transmittance we want will not likely have sufficient strength to withstand these pressures without additional support to reduce the area to be spanned. This project aims to fabricate a membrane that will provide the necessary support.

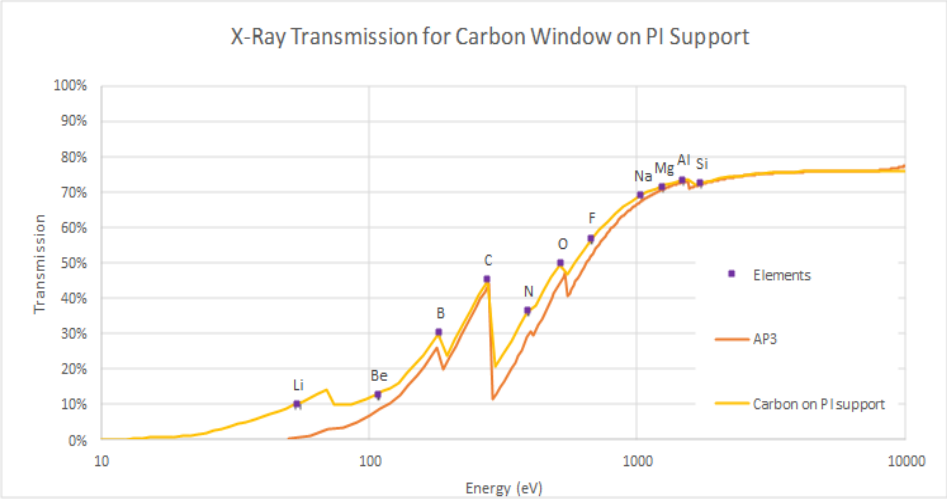


Figure 1.4 X-ray transmission for a current polymer-based window (AP3), and a hypothetical carbon-based window with the proposed polyimide support structure (for example, similar to Fig 1.1). The transmission tops out around 75% for higher energies because of the thicker silicon ribs in the window (see Fig 1.1b). Although the transmission is better at lower energies, it could be improved by increasing the open area in the support structure. Because of time constraints, this was not attempted in this project. Transmission data courtesy of the Center for X-Ray Optics at Lawrence Berkeley National Labs.

1.3 Support Membrane

The support membrane should be sufficiently strong, while not blocking so much signal that it defeats the purpose of the thinner window. We use a thin film for the support membrane (about 300 nm thick) so that higher energy x-rays still transmit well through it. By fabricating nanopores into the film, the leak-tight portion of the window would only need to span across the pores, and thus could be thin enough for better transmission (Fig 1.4). Polyimide is a high-strength polymer that can be readily manipulated using microfabrication techniques [4], and thus was a good choice for our purposes.

Other groups have made polyimide membranes similar to the proposed support structure. Van Rijn did extensive work developing and characterizing perforated and unperforated films [5]. He specialized in microsieves (membranes with pores on the same order as film thickness) made from

various materials, including polyimide [4]. The techniques he developed for fabricating and testing microsieves formed a foundation for hosts of similar work, including ours.

Olga Makarova et al. [6] made a nanofilter from a 25 um polyimide film with 250 nm pores. Their pores were very precisely sized and had highly vertical side walls. Keping Han et al. [7] made a 600 nm thick polyimide film with 200 nm pores also for filtration. The pores resisted deformation up to pressures of 1.71 atm, although it was not clear whether deformation was tested above that pressure. Both applications were in filtration, but the films demonstrated promising durability and strength.

In this project, electron beam lithography, thermal deposition, and reactive ion etching transfers arrays of pores into submicron thick polyimide (Fig 1.2). This configuration could support an ultra-thin leak-tight layer, allowing for greater x-ray transmission. After being released from the substrate, the membrane's strength was tested using the bulge testing method.

Chapter 2

Methods

2.1 Fabrication Overview

Beginning with 300 nm thick polyimide on a silicon wafer, the sample is coated with electron beam resist and exposed in an SEM to create hexagonal hole arrays. After depositing a nickel hard mask onto the surface of the resist, the holes are transferred into the polyimide by reactive ion etching. The hard mask is removed by dissolving the resist in a solvent. The film is then released from the silicon substrate and sandwiched between adhesive-backed washers in preparation for bulge testing. The process is diagrammed in Fig 2.1.

2.2 Substrate

The process begins with 300 nm thick polyimide on a silicon wafer. This arrangement is a standard substrate provided by Moxtek. Because electron beam lithography can only pattern small areas in a reasonable amount of time, the wafer is cleaved into smaller pieces. The wafer is first coated with AZ 3330 photoresist to protect the substrate surface from the debris caused by cleaving. Using the diamond scribe, the wafer is cleaved into chips about 1.5 cm x 1.5 cm. Removing the photoresist

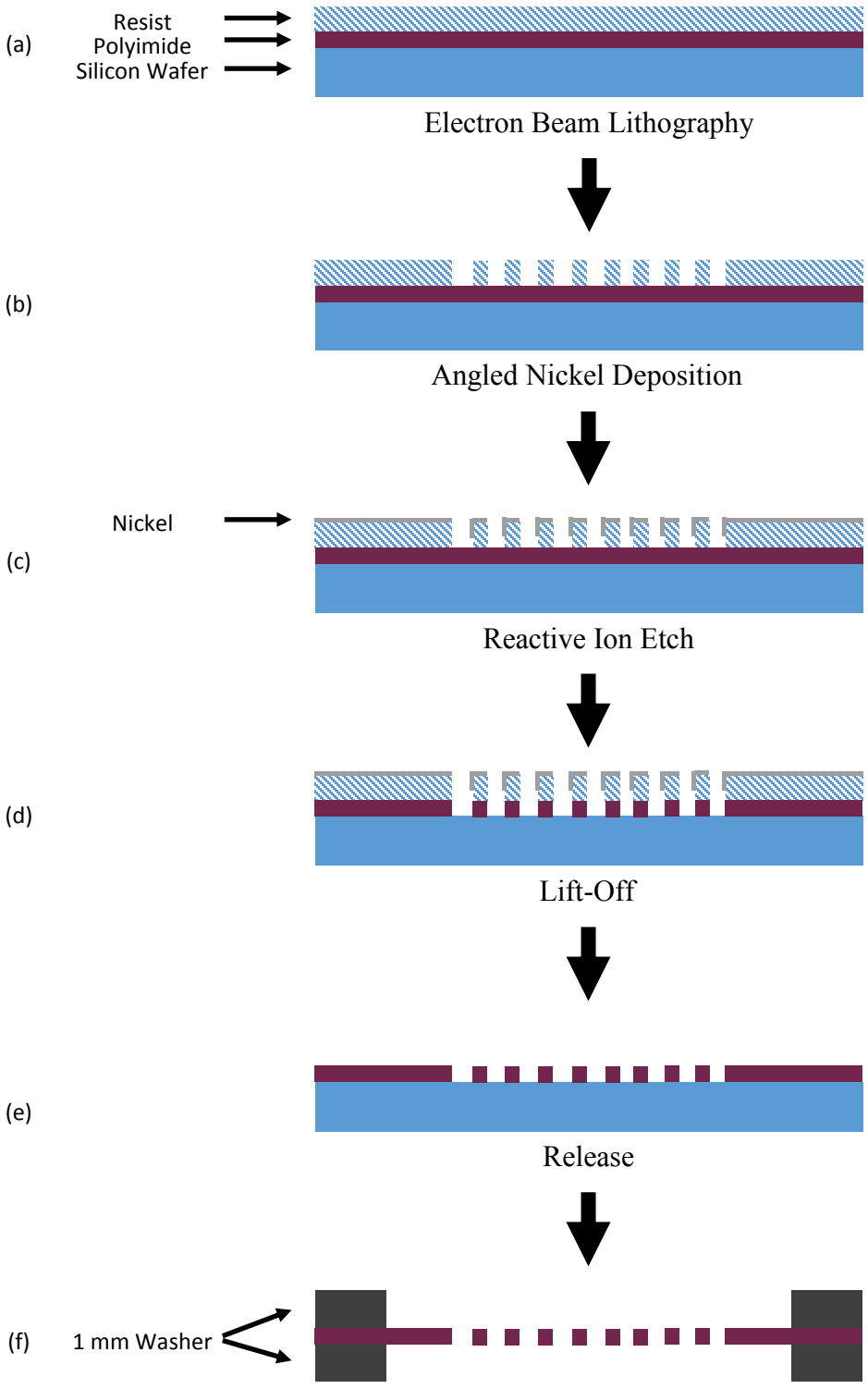


Figure 2.1 Process overview for fabricating a 300 nm thick porous membrane.

with acetone and then rinsing with isopropyl alcohol cleans the sample surface from any residue. This yields small, clean, polyimide coated samples that are ready for further processing.

2.3 Electron Beam Lithography

Electron beam lithography creates features and patterns by exposing an electron-sensitive polymer, the electron beam resist, to high energy electrons (about 30 keV) inside an SEM. When electrons hit the resist, they change the chemical structure, making the exposed areas more soluble in the developer solution. By exposing specific areas and developing them away, nanoscale features can be made in the resist.

Our 200 nm pore size required that we use electron beam lithography because it can create features at sizes that are unavailable to conventional photolithography. Photolithography is limited by diffraction; features similar in size to the light's wavelength cannot be resolved because the light diffracts around them. Because electrons have a much smaller wavelength, electron beam lithography does not have this problem. Unfortunately, electron beam lithography is time-consuming, and thus not an economically viable manufacturing process. However, it works well for demonstrating proof of concept, and more advanced techniques such as laser interference lithography (beyond the scope of this thesis) may be used for possible future commercial applications.

The electron beam resist (ZEP 520-A) is applied to the samples by dripping it on, then spinning the substrate at 2000 rpm for 60 seconds, yielding a 700 nm thick resist layer across the whole chip (see Fig 2.1a). The pattern was created with DesignCAD housed within the Nanometer Pattern Generation System (NPGS) software from JC Nabity Lithography Systems. Multiple 100 μm x 100 μm hexagonal arrays of 200 nm pores with 400 nm pitch were written with the FEI XL30 ESEM in the MacDonald Building. The amount of exposure to electrons, or dosage, is set by how long the beam stays in a specific spot. To determine the correct dwell time, a set of patterns was

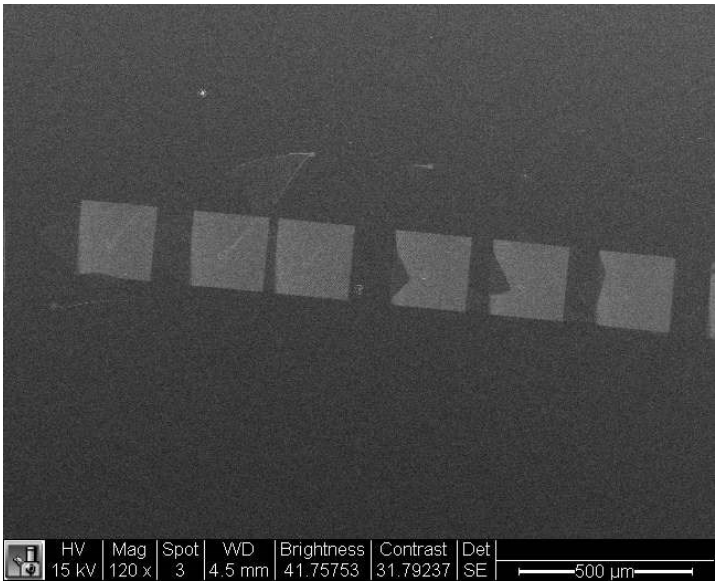


Figure 2.2 An example dose test, lower dosages on the left. These patterns were 200 µm x 200 µm, as opposed to the 100 µm x 100 µm used for eventual bulge testing. In this dose test, the spacing was set to be 100 µm; the observed irregularity is due to stage movement. In the patterns used for bulge testing, the spacing was 1.5 mm so that multiple patterns could be released from the substrate.

written at varying dosages. Doses that were too low gave holes smaller than desired, and doses too high yielded holes too big. An example of a dose test is shown in Fig 2.2.

Writing pattern areas much larger than 100 µm x 100 µm resulted in hole deformation on the edges, therefore areas larger than this were difficult to obtain. Putting multiple 100 µm x 100 µm patterns together was limited by the unreliability in stage movement; setting the patterns too close together frequently resulted in overlaps. Therefore, only individual 100 µm x 100 µm areas were patterned and tested. Patterns were spaced by 1.5 mm so that multiple patterns could be released from each sample.

Development was carried out in the cleanroom. The sample was placed in the developer (ZED-N50) for 90 seconds, transferred to a rinse (ZMD-D) for 15 seconds, then rinsed with deionized water for 60 seconds. It is important that these solutions are replaced regularly for consistent results: every three samples proved to be a safe choice. It was then descumed (i.e. had residual

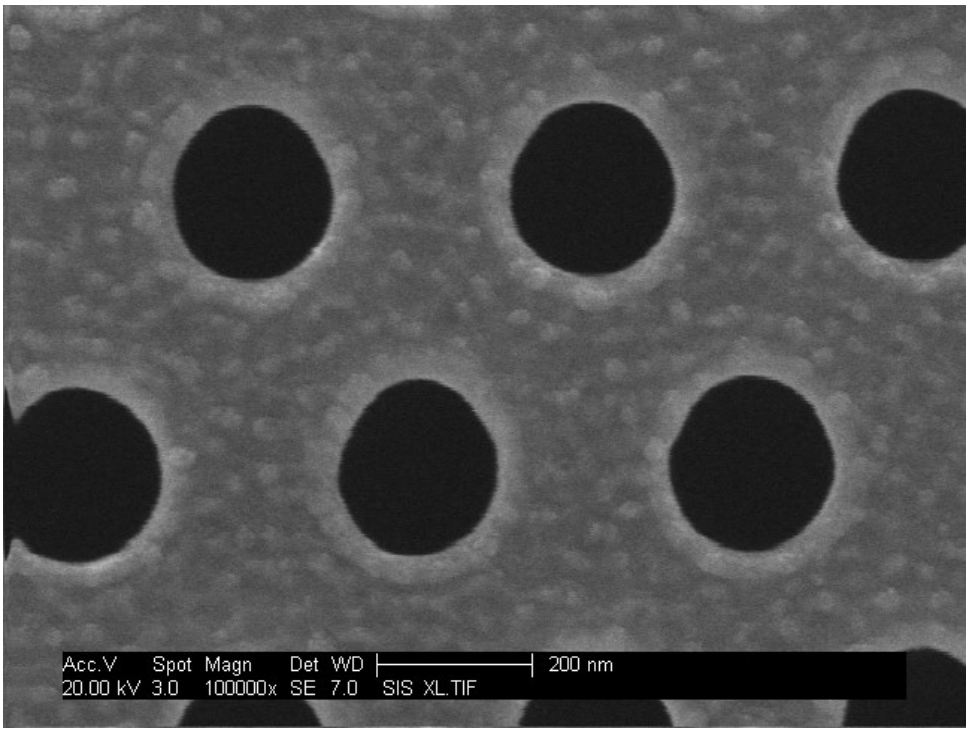


Figure 2.3 Holes in the resist after lithography and development, before nickel deposition. The surface roughness is from the 15 nm Au/Pd coating for imaging.

resist removed) in an oxygen plasma etcher (PlanarEtch II) at 100 W for 60 seconds. At this point, the pattern is in the resist, but not yet in the polyimide (see Fig 2.1b and Fig 2.3).

2.4 Thermal Evaporation

Transferring the patterns to the polyimide requires reactive ion etching. However, the etch process also attacks the resist at a rapid rate, fast enough to etch the polyimide in areas that we want protected. Clearly, the resist was inadequate as an etch mask. Therefore, we first deposit a thin, highly etch resistant layer, or hard mask, on the surface of the resist. Nickel has a reactive ion etch rate that is practically zero and is a metal that we already deposit in our thermal evaporator (Jim, in the underground lab), making it a great hard mask candidate for this project.

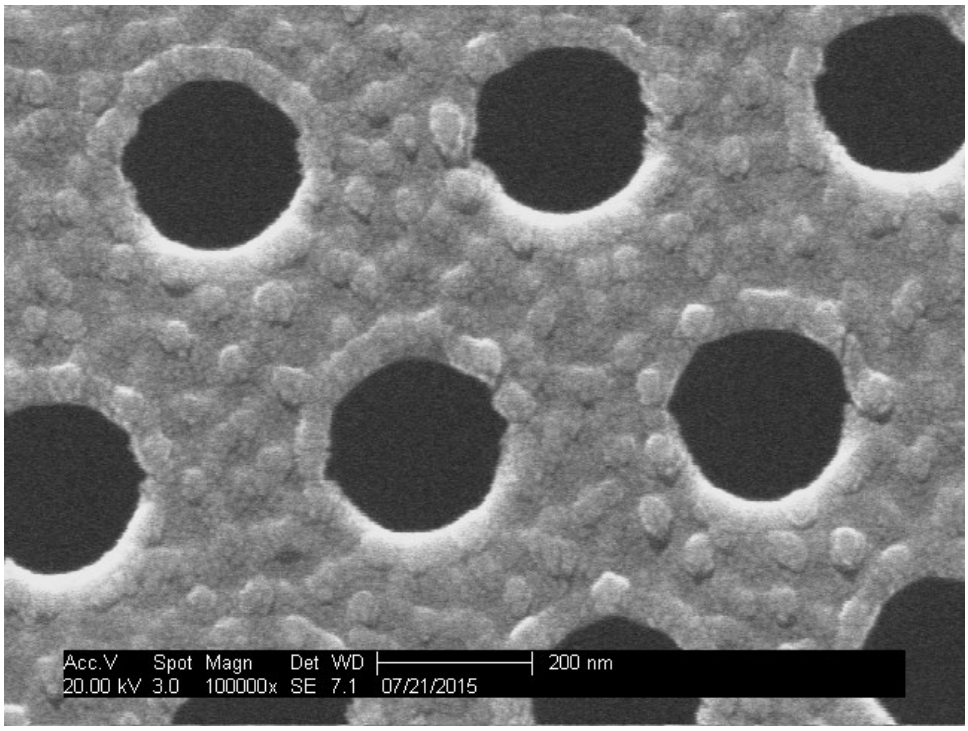


Figure 2.4 Nickel hard mask before reactive ion etching. The nickel is 15 nm and was deposited at an angle such that only the surface and part of the side walls are coated.

Thermal evaporation coats a substrate by heating a source material in high vacuum until it begins to expel atoms from the surface. When the ejected atoms hit the substrate, they stick. By placing a crystal monitor in the chamber and measuring the resonant frequency shift as material coats it, the process can precisely deposit nanometer thick layers.

Pure nickel is placed in a highly resistive alumina-coated tungsten boat. The sample is mounted above the boat at a 45° angle. This allows the nickel to deposit only on the resist surface and sidewalls, leaving the polyimide inside the holes exposed. The chamber is pumped down to high vacuum, and current applied to the boat is slowly ramped up until the deposition rate is greater than 1 Å/sec. The shutter shielding the substrate is then opened until 15 nm of nickel deposits on the sample. Now there is a 15 nm nickel hard mask on the surface and some of the sidewalls of the resist, leaving the target polyimide uncovered (see Fig 2.1c and Fig 2.4).

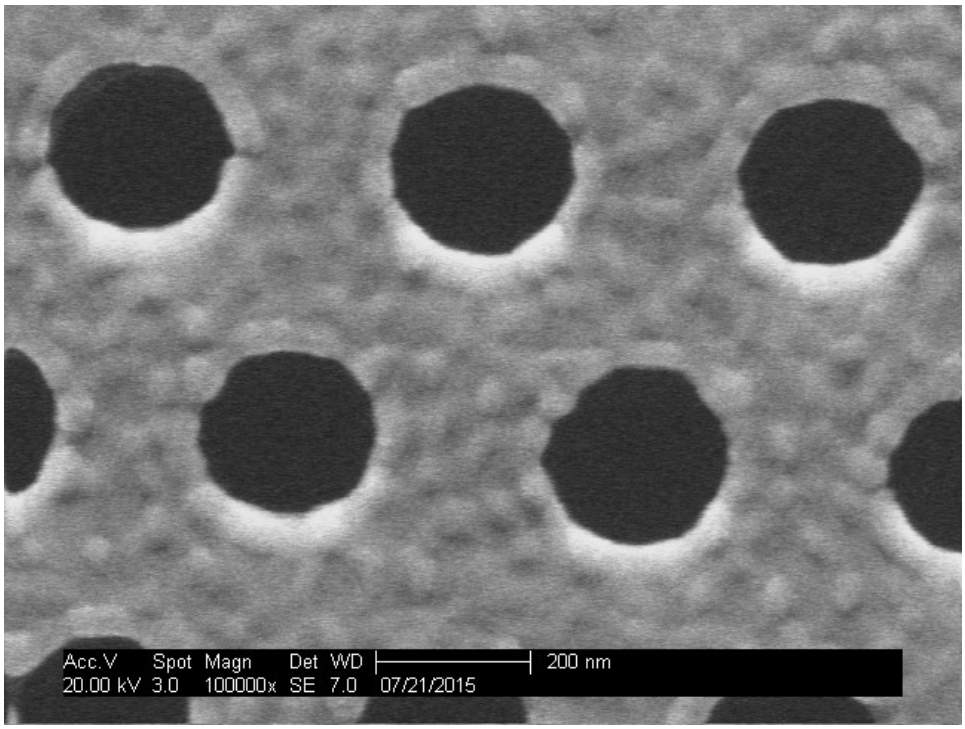


Figure 2.5 Sample surface after reactive ion etching and before resist removal. The nickel mask is slightly smoother than before the RIE step.

2.5 Reactive Ion Etching and Resist Removal

Reactive ion etching removes material from samples both by bombardment and chemical reaction. Gas flows into a vacuum chamber and is ionized by a strong radiofrequency (RF) electromagnetic field. Voltage applied to the set of parallel plates at the top and bottom of the chamber creates a strong electric field that accelerates the ions toward the sample. The resulting collisions and reactions provide a very anisotropic (i.e. directional) etch in areas not protected by a hard mask.

The polyimide was etched using 10 sccm O_2 and 3 sccm CF_4 at 300 W of RF power and 60 mTorr for 1 minute 40 seconds. This transfers the hole pattern into the polyimide (see Fig 2.1d). An SEM image of the sample at this point is shown in Fig 2.5. Etching for too long resulted in widening of the pores, yielding pores that were too large or that overlapped. Too short an etch time did not allow the process to etch all the way through the polyimide.

(a) (b)

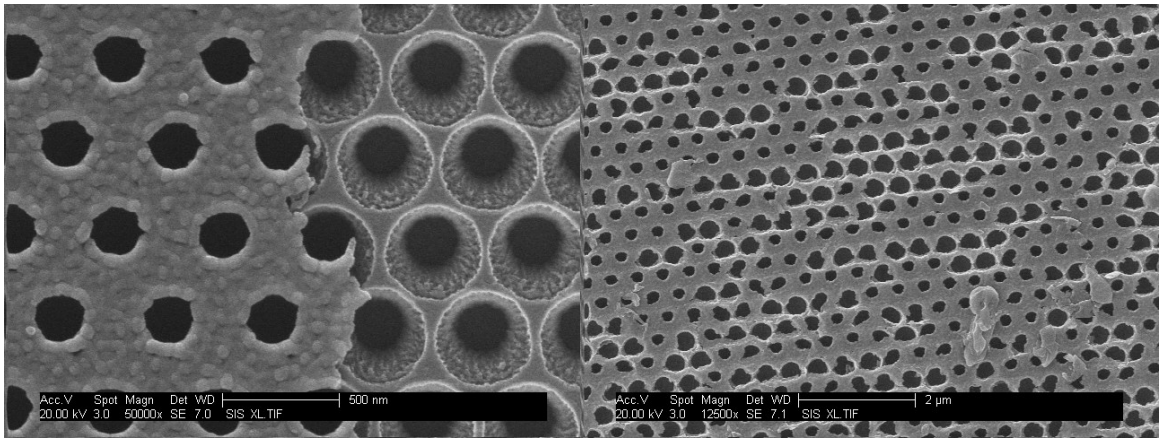


Figure 2.6 When fresh NMP is not used, not all of the resist is removed and a residual layer of nickel and resist remains. The residual layer may just be a section of the mask that stuck, or it may just look messy. In (a), the nickel has held together well (in part possibly because 33 nm of nickel was deposited on the sample shown instead of 15 nm), and the mask pattern is apparent. It also shows the widening due to the reactive ion etch. The sample in (b) left a much messier residue. Both samples were coated with about 15 nm of Au/Pd prior to imaging.

It should be noted that the RIE was not perfectly anisotropic, and etching for any amount of time widened the pores (see Fig 2.6a). Therefore, to get the correct pore size, the lithography dose was lowered such that the diameter of the holes after etching was 200 nm. This widening effect may also have played a role in the sloped pore channels (see Fig 3.3).

Now that the pore arrays were in the polyimide, the resist and nickel hard mask needed to be removed. The sample soaked in *N*-Methyl-2-pyrrolidone (NMP) for at least 6 hours (extra time made no noticeable difference) to dissolve the resist, removing the nickel with it. It is vital to use fresh NMP, otherwise residual resist will remain in the patterned areas (see Fig 2.6). Sonication destroyed the polyimide layer and was not necessary for complete removal of the resist when fresh NMP was used. After rinsing with water under a slow stream, the sample is now a porous polyimide film on a silicon substrate (see Fig 2.1e and Fig 3.2).

The patterned polyimide was released from the wafer using Moxtek's proprietary standard

process. This leaves the film weakly attached to the substrate. An adhesive-backed washer with 1 mm inner diameter is placed on the film, centered on one of the hole arrays. Setting the washer correctly was very difficult, and methods to facilitate this should be explored if attempted in the future. After cutting around the washer, it is lifted off, and a second washer is placed opposite the first to sandwich the patterned membrane (see Fig 2.1f).

2.6 Bulge Testing

Bulge testing reveals material properties by applying an excess pressure to one side of a membrane and measuring the resulting displacement height across the middle of the film. The bulge data are fitted to a circle. From the circle fit, relevant material properties such as the internal stress σ and Young's modulus E can be calculated [8]. σ quantifies the force per unit area exerted by the molecules on each other and is found by

$$\sigma = \frac{pR}{2t},$$

where p is the pressure, R is the membrane's radius of curvature as it bulges, and t is the membrane thickness [8] (see Fig 2.7). The ultimate tensile strength σ_{ts} is found by calculating the stress at the last pressure before breaking and gives an idea of how much force a material can handle. Strain ε is the ratio of the change in length to the original length as force is applied to a material. In bulge testing, it is found by

$$\varepsilon = \frac{2w_0^2}{3a^2},$$

where w_0 is the measured height of the membrane, and a is the washer's inner radius. E is a property that describes material stiffness (high E means high stiffness) and is found by

$$E = (1-\nu)\frac{3pa^4}{8tw_0^3},$$

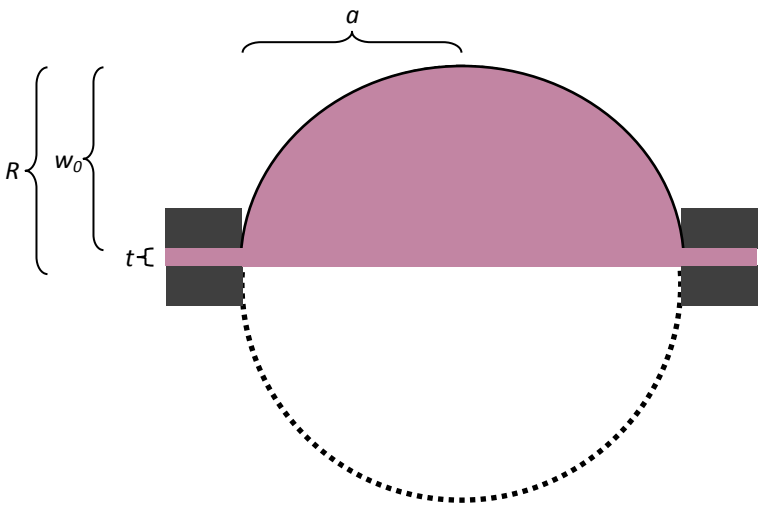


Figure 2.7 Diagram of the terms used in bulge testing calculations. R is the radius of the circle fitted to the membrane bulge, w_0 is the height of the membrane, t is the thickness of the membrane, and a is the inner radius of the washer.

[8] where ν is Poisson's ratio (the ratio of how much a material shrinks in one direction to how much it is stretched in the other direction, our lab used 0.22 for polyimide, although 0.33 may be more correct). E can also be calculated as the slope of the stress-strain curve, which is how it was obtained here (see Fig 3.6).

The membrane height is measured by detecting the diffuse reflection of a laser shining on the membrane surface (see Fig 2.8). The detector gives the height of the membrane based on the position of the peak intensity on the detector. Because 300 nm thick polyimide membranes are transparent, we needed a way to create a diffuse reflection without changing the strength of the film. To accomplish this, the surface was coated with 200 nm silver colloids to scatter the incident light. The coating was applied by placing the sample on a hotplate, spraying the membrane with colloidal silver solution, letting it dry on a hotplate, and then repeating until a diffuse reflection was obtained. The colloids were not expected to influence the measurements of the film's strength.

The sample was then mounted and clamped in the bulge testing apparatus. The laser scanned across the membrane at 20 μm/sec at each pressure step. Following each pass of the laser, the

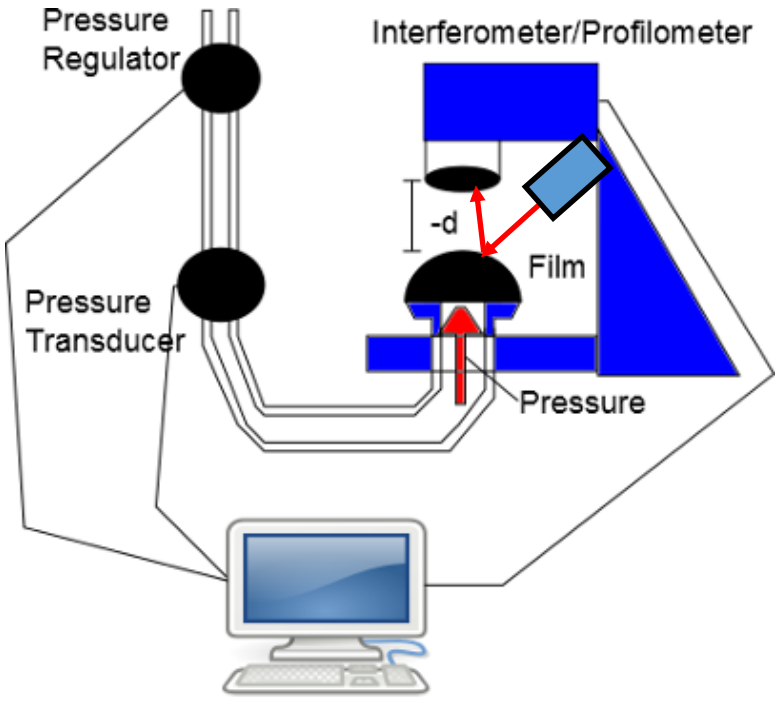


Figure 2.8 The bulge height is measured across the middle of the membrane as pressure is applied below. The computer tells the regulator what pressure to apply, the transducer tells the computer what it's actually giving, and the height across the middle of the film is measured by the optical profilometer. The radius of the circle fit with the associated pressure is used to calculate the stress and strain in the film. Diagram used with permission of Joseph Rowley.

pressure was increased by 0.5 psi. This continued until the membrane burst.

Chapter 3

Results

3.1 Patterned Film

Many films were patterned and taken through the process up until the release step, until we were confident in the reliability of creating the pores in the polyimide. We attempted to release patterns from three samples, but, owing to the difficulty of aligning the washer with the pattern and the ease of tearing the membranes, only four films from two samples were successfully released onto 1 mm inner diameter washers. Sample1a had the pattern close to the edge of the washer (see Fig 3.1a); Sample1b had the pattern close to the middle (see Fig 3.1b); and Sample1c and Sample2 were from unpatterned regions of the samples. Sample1a, Sample1b, and Sample1c were from the same substrate.

Imaging showed that the intended pattern indeed was transferred to the polyimide film. The pores are arranged in a single 100 μm x 100 μm hexagonal array with the pore size varying <10% of the mean. The images of the pattern from the top (Fig 3.2) and of the cross-section (Fig 3.3) show that the pore walls are not strictly vertical. The bottom diameter was about 210 nm and the top was about 306. From this, the slope of the sidewalls can be estimated to be about 6:1. While

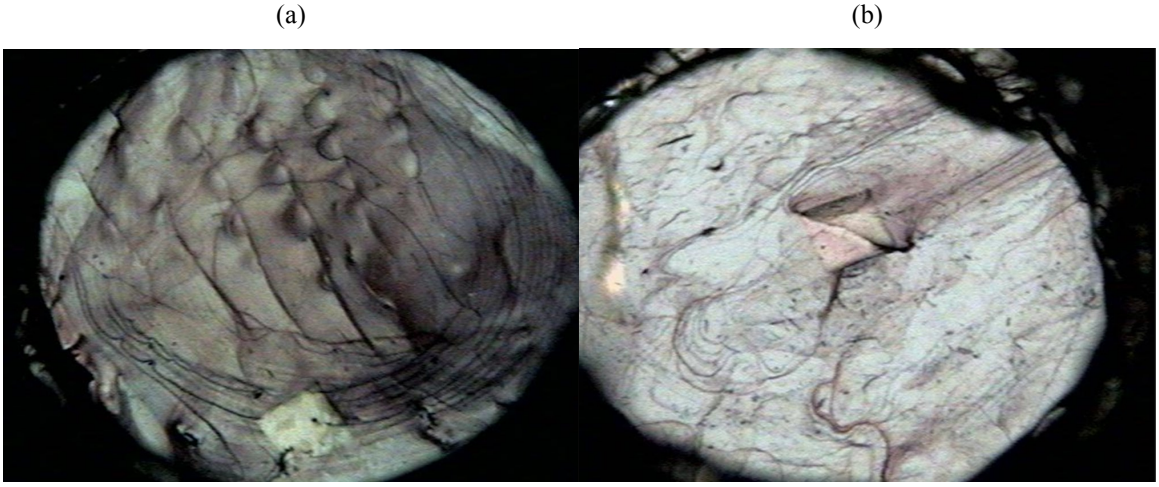


Figure 3.1 Backlit, optical images of Sample1a (a) and Sample1b (b) after colloidal silver coating and before bulge testing. The pattern in Sample1a is the square located close to the bottom of the membrane, and the pattern in Sample2a is the square close to the middle of the membrane. The lines observed come from multiple applications of colloidal silver solution. As the droplets dried, silver colloids tended to move toward the edges, an effect known as the coffee effect [9].

for the current project we assumed this to not be a major problem, this may affect strength and transmission models in unknown ways, and should be taken into account in future work.

3.2 Bulge Testing Results

The samples used for bulge testing had area dosages from 40 - 130 $\mu C/cm^2$. The spread of dosages accounted for possible variation in lithography writing conditions and ensured obtaining at least one good pattern. Ultimately, the 90 $\mu C/cm^2$ (Sample1a) and 130 $\mu C/cm^2$ (Sample1b) patterns were released for bulge testing.

All four membranes were taken to bursting. The patterned membranes appeared to break through the patterned area, as expected (see Fig 3.4). The burst pressures and calculated material properties are shown in Table 3.1. For comparison, the σ_{ts} and E for steel are 860 MPa and 180 GPa respectively, and σ_{ts} and E for bulk polyimide range from 152-390 MPa and 2.5-8.5 GPa

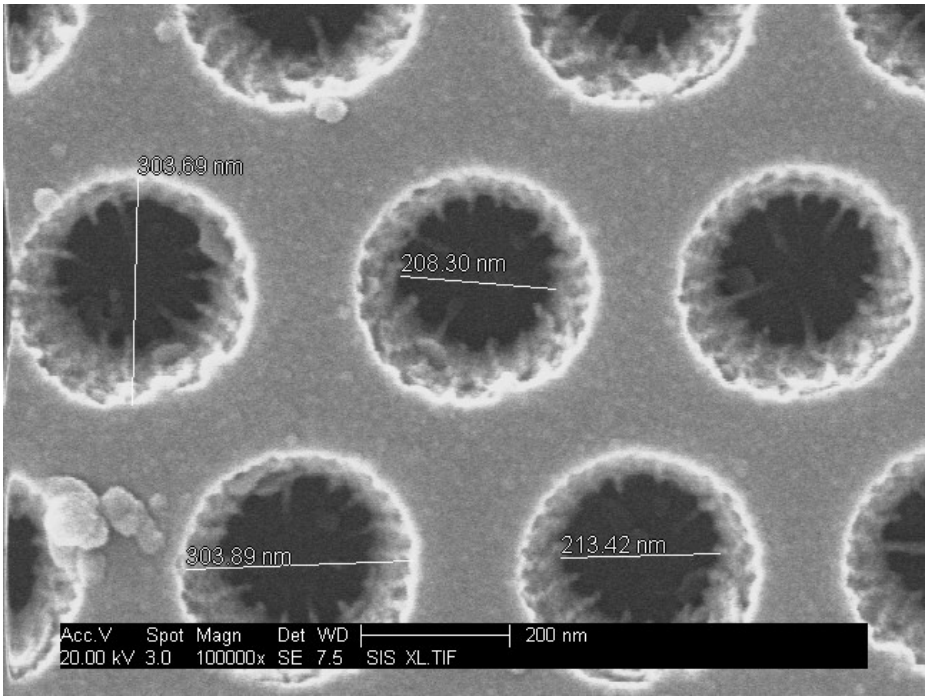


Figure 3.2 Top view SEM image of finished patterned polyimide film just before release from the substrate. From Sample1a (90 $\mu C/cm^2$). The sample was coated with about 15 nm of Au/Pd prior to imaging.

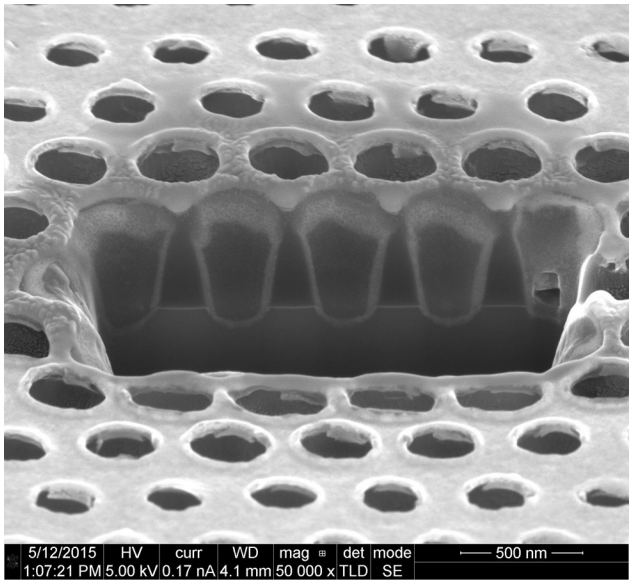
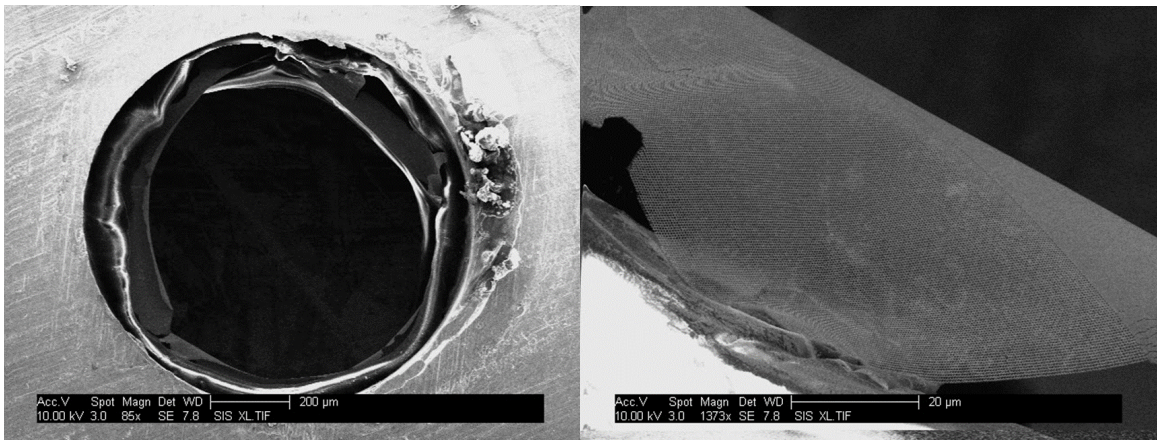


Figure 3.3 Cross section view of the polyimide film before after processing but still on the substrate. A section of the film was milled away with the focused ion beam in the FEI Helios Nanolab 600 and imaged at 52°. The image illustrates the slanted pore channels. The sample was coated with about 15 nm of Au/Pd prior to imaging.

respectively [10]. Only one E and one σ_{ts} were able to be calculated because measuring the bulge height was unreliable. It should also be noted that even the measurements that were obtained are not particularly reliable either. Although the colloidal silver created a diffuse reflection, a significant amount of light was able to pass through the film, reflect back, and create false signals in the detector. This resulted in an artifact layer of data points that ruined the circle fit (see Fig 3.5a). To get σ_{ts} for Sample1b, it was necessary to delete all the artifact data at the last pressure step, leaving just enough points for a rough circle fit (see Fig 3.5b). Therefore, the σ_{ts} should be considered a preliminary estimate. In the data for Sample1a, there were no good points left close to the breaking pressure. Sample1a had artifact-free data up until about 16.5 psi, which gave enough points on the stress-strain curve to calculate E (see Fig 3.6). Once again, the spread of data points and lack of repeated trials indicate that this is a rough preliminary result. Sample1b did not have enough artifact-free data to calculate E. Neither of the blank samples had clean enough data for either

(a) (b)



(c)

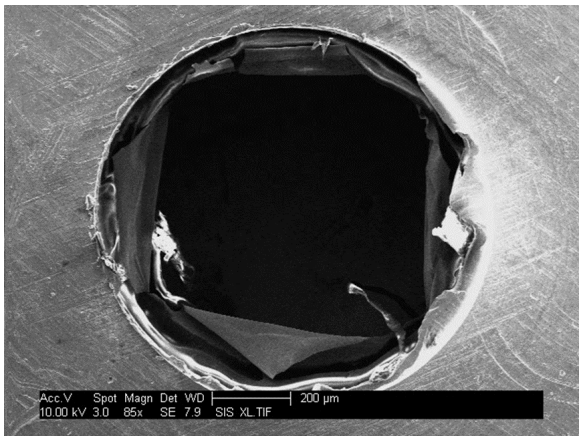
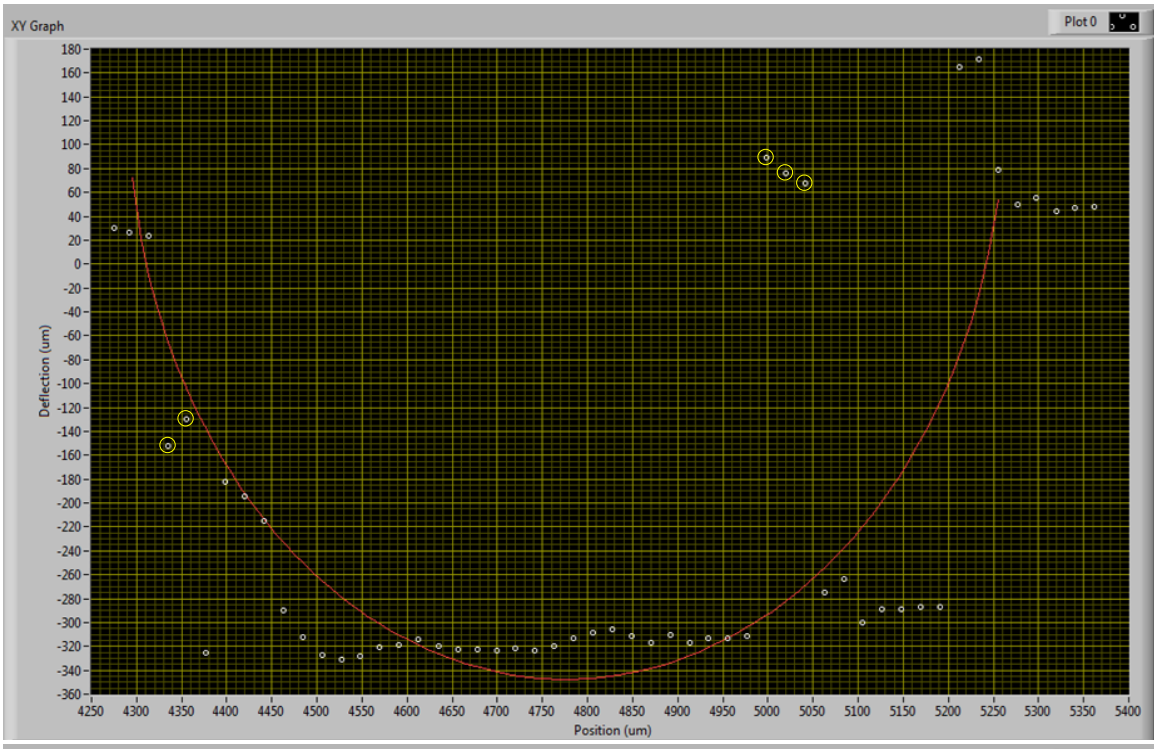


Figure 3.4 (a) Sample1a after bulge testing. (b) Sample1a, patterned area. As would be expected, the membrane broke through the pattern. (c) Sample1b after bulge testing. The patterned areas were unable to be located in Sample1b.

σ_{ts} or E to be easily calculated; artifacts would need to be removed from many pressure steps to calculate E.

Given its significantly lower burst pressure, it's possible that Sample2 had undetected defects. The pattern location within the membrane may also have affected the bursting pressure. Sample1b had the pore array in the center of the washer area, whereas Sample1a had it closer to the edge. If the stress was concentrated closer to the edges, then the weaker porous area would reach maximum

(a)



(b)

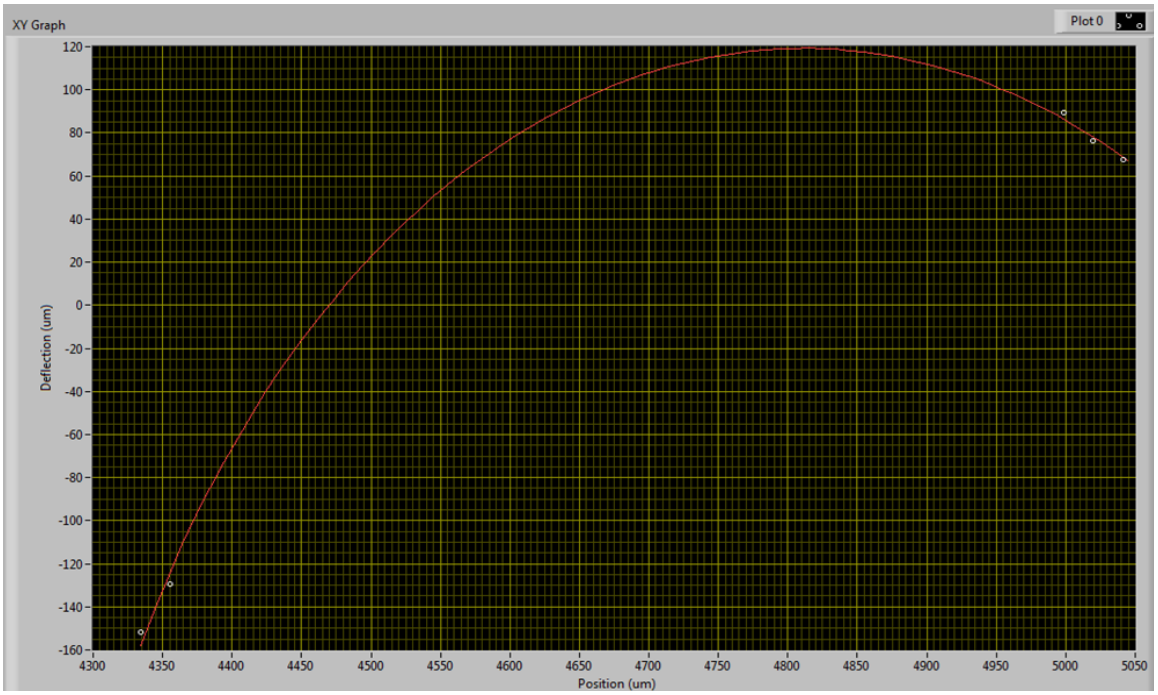


Figure 3.5 (a) Raw data from the last pressure step before breaking (35 psi) for Sample1b. The excess pressure is from below, so the membrane is bulging upward. The flat sets of points on either end are the washer, the circled points are believed to be from the actual membrane. The other points are believed to be artifacts from reflections. The circle fit (red line) clearly does not fit the membrane. (b) Same set of data with the non-membrane points removed.

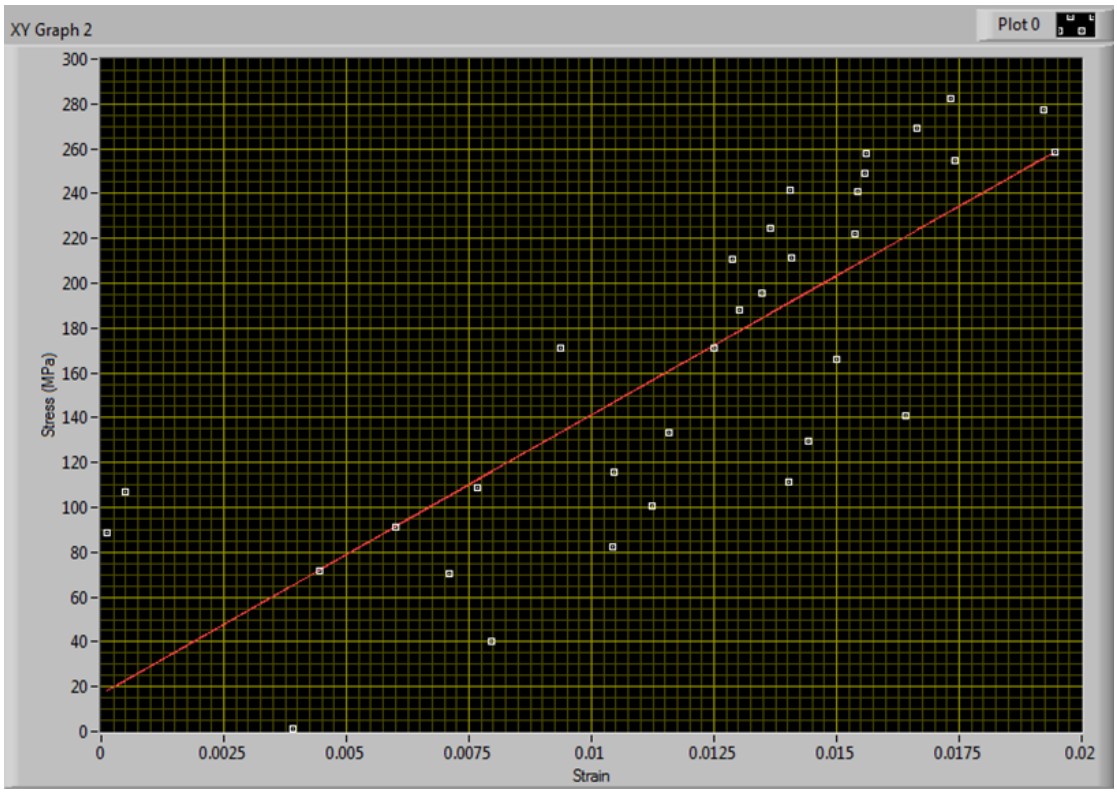


Figure 3.6 Stress-strain curve (red line) for Sample1a. The Young's modulus is the slope of the line. The stress-strain data points are calculated from the radius of the film's bulge at each given pressure. The data shown is for pressures from 0 psi to 16.5 psi; beyond 16.5 psi, the bulge height data used to calculate the radius contained signals from reflections that ruined the circle fit. The error bars in this data are large, and the E calculated from it should be regarded as a low-confidence level preliminary result.

Table 3.1 Burst Pressure, calculated Young's modulus E, and calculated ultimate tensile strength σ_{ts} from bulge testing for the various films. The extracted material properties should be taken to be very rough estimates with low confidence levels, and empty spaces indicate a lack of sufficient data.

Film	Burst Pressure (psi)	Burst Pressure (atm)	E (GPa)	σ_{ts} (MPa)
Sample1a (90 $\mu C/cm^2$)	27	1.84	9.7	
Sample1b (130 $\mu C/cm^2$)	35.5	2.42		220
Sample1c (Blank)	81.5	5.55		
Sample2 (Blank)	32.5	2.21		

stress at a lower pressure than if it were in the middle of the membrane, causing it to break earlier.

3.3 Conclusions and Future Work

The membrane strength results, though far from conclusive, may be promising for future application to x-ray windows. Patterned samples successfully withstood the benchmark pressures, and while array shape and size were not exactly representative of what the final window configuration may be, the burst pressures obtained are an encouraging indicator. Sample1b in particular surpassed the 2 atm benchmark, showing that this configuration could deserve further attention. These results indicate that thin polyimide membranes with high porosity may be able to serve as a support structure for an ultra-thin transmissive window.

The tests done here need to be repeated many more times to obtain trustworthy results. Future investigations may also improve bulge height detection and thus obtain more reliable material properties. As stated earlier, bulge height measurement was affected by stray reflections. However, these reflections usually occurred close to the bottom of the detector's range, so it may be possible

to eliminate them by raising the detector height such that those reflections are below the range of the detector. In these experiments, adjusting the detector higher resulted in significant signal loss from the membrane; however, more uniform application of colloidal silver or adjustment in detector parameters may prevent loss of data. With these difficulties reduced, more data could be obtained for greater confidence.

The fabrication process could also be applied to a wide variety of patterns, allowing for investigation of optimal porosity, pore distribution, and pore shape. More experimentation with transmission modeling could reveal optimal porosity, pore distribution, pore shape, and thickness parameters. The fabrication process developed here could be used to create such films for testing. With further work, membranes of this type could be effective support structures in a more transmissive x-ray window.

Index

beryllium, 2, 3
bulge testing, 6, 7, 15, 16, 19

descum, 10
developer, 10

electron beam lithography, 6, 9
electron microscope, 1, 9
etch, 11, 13

filtration, 6

graphene, 3

Han, 6

lithium, 2, 3

Makarova, 6

nickel, 12, 14
NMP, 14
NPGS, 9

photoresist, 7
Poisson's ratio, 16
polyimide, 5, 7, 11–14, 16, 18

reactive ion etching, 6, 7, 13
release, 14
resist, 7, 9, 11, 12, 14

silver colloids, 16
strain, 15, 17, 21, 24
stress, 15, 17, 21, 24

thermal evaporation, 6, 12

ultimate tensile strength, 15, 25

Van Rijn, 5

x-ray detector, 1
x-ray spectroscopy, 1
x-ray window, 3, 5

Young's modulus, 15, 21, 24, 25

List of Figures

1.1 Proposed Window Schematic 2

1.2 Support Structure Schematic 3

1.3 Beryllium Window Transmission Curve 4

1.4 AP3 and Proposed Window Transmission Curves 5

2.1 Process Flow Diagram 8

2.2 Dose Test SEM Image 10

2.3 Sample Directly After Lithography, Before Nickel Deposition, SEM Image 11

2.4 Sample Directly After Angled Nicke Deposition, SEM Image 12

2.5 Sample After RIE, Before Resist Removal 13

2.6 Residue Layer After Poor Resist Removal 14

2.7 Bulge Testing Terms Diagram 16

2.8 Bulge Testing Diagram 17

3.1 Washer-Mounted Patterned Membranes, Pre-Bulge Testing 19

3.2 Pattern Top View SEM Image 20

3.3 Pattern Cross Section SEM Image 21

3.4 Burst Films 22

3.5 Bulge Test Data - Circle Fit 23

3.6 Bulge Test Data - Stress-Strain Curve 24

Bibliography

[1] F. Scholze and M. Procop, "Detection efficiency of energy-dispersive detectors with low-energy windows," X-Ray Spectrometry **34,** 473–476 (2005), pT: J; CT: European X-Ray Spectrometry Conference; CY: JUN 06-11, 2004; CL: Alghero, ITALY; UT: WOS:000233349100001.

[2] R. Perkins, D. Allred, L. Knight, and J. Thorne, "Design of high performance soft x-ray windows," Advances in X-Ray Analysis **33,** 615 (1990).

[3] S. Huebner, N. Miyakawa, S. Kapser, A. Pahlke, and F. Kreupl, "High Performance X-Ray Transmission Windows Based on Graphenic Carbon," IEEE Transactions on Nuclear Science **62,** 588–593 (2015).

[4] C. van Rijn, "Chapter 6 Polymeric membranes," Membrane Science and Technology **10,** 133–167 (2004).

[5] C. van Rijn, "Chapter 5 Membrane deflection and maximum pressure load," Membrane Science and Technology **10,** 111–131 (2004).

[6] O. Makarova, C. Tang, P. Amstutz, M. Hoffbauer, T. Williamson, R. Divan, and A. Imre, "Fabrication of high density, high-aspect-ratio polyimide nanofilters," In *The 53rd Intl. Conf. on Electron, Ion, and Photon Beam Technology and Nanofabrication*, (2009).

[7] K. Han, W. Xu, A. Ruiz, P. Ruchhoeft, and S. Chellam, "Fabrication and characterization of polymeric microfiltration membranes using aperture array lithography," Journal of Membrane Science **249,** 193–206 (2005).

[8] J. Vlassak, Ph.D. thesis, Stanford University, 1994.

[9] K. Sensinig, "The Coffee Ring Effect - Intriguing Microscopic Video,", 2011.

[10] DuPont and HD-MicroSystems, 2016.